"Characterization of Quasi-Stationarity Regions for Vehicle-to-Vehicle Radio Channels"

He, Ruisi ; Renaudin, Olivier ; Kolmonen, Veli-Matti ; Haneda, Katsuyuki ; Zhong, Zhangdui ; Ai, Bo ; Oestges, Claude

Abstract

We analyze the nonwide-sense-stationarity (nonWSS) of vehicle-to-vehicle (V2V) radio channels using three metrics: 1) the correlation matrix distance (CMD); 2) the wideband spectral divergence (SD); and 3) the shadow fading correlation. The analysis is based on measurements carried out at 5.3 GHz using a 30 × 4 MIMO system in suburban, urban, and underground parking areas. Several factors such as the existence of a line-of-sight (LOS), the speed of cars, and the antenna array size and configuration are considered in the analysis of non-WSS. It is found that quasi-stationarity region ranges from 3 to 80 m in different V2V scenarios, and is strongly affected by the above factors. Based on the comparison of the equivalent quasi-stationarity region size estimated by the three metrics, it is suggested to use SD and shadowing correlation metrics for systems with small electrical array apertures and to use CMD metric only for arrays with large electrical apertures.

Document type : *Article de périodique (Journal article)*

This article has been accepted for publication in a future issue of this journal, but has not been fully edited. Content may change prior to final publication. Citation information: DOI 10.1109/TAP.2015.2402291, IEEE Transactions on Antennas and Propagation

Characterization of Quasi-Stationarity Regions for Vehicle-to-Vehicle Radio Channels

Ruisi He, *Member, IEEE*, Olivier Renaudin, Veli-Matti Kolmonen, Katsuyuki Haneda, *Member, IEEE*, Zhangdui Zhong, Bo Ai, *Senior Member, IEEE*, and Claude Oestges, *Senior Member, IEEE*

***Abstract*—We analyze the non-wide-sense-stationarity (non-WSS) of vehicle-to-vehicle (V2V) radio channels using three metrics: the correlation matrix distance (CMD), the wideband spectral divergence (SD), and the shadow fading correlation. The analysis is based on measurements carried out at 5.3 GHz using a 30×4 MIMO system in suburban, urban, and underground parking areas. Several factors such as the existence of a line-of-sight (LOS), the speed of cars, and the antenna array size and configuration are considered in the analysis of non-WSS. It is found that quasi-stationarity region ranges from 3 to 80 m in different V2V scenarios, and is strongly affected by the above factors. Based on the comparison of the equivalent quasi-stationarity region size estimated by the three metrics, it is suggested to use SD and shadowing correlation metrics for systems with small electrical array apertures and to use CMD metric only for arrays with large electrical apertures.**

***Index Terms*—Correlation matrix distance, quasi-stationarity region, shadowing, spectral divergence, vehicle-to-vehicle channels.**

I. Introduction

VEHICLE-TO-VEHICLE (V2V) communication networks will potentially improve the efficiency and safety of Intelligent Transportation Systems (ITS). The grand vision of ITS is that all road users gather sensor data about traffic and road state information, share information for safety improvements, and thus prevent traffic accidents by periodically monitoring the locations of surrounding vehicles [2]. Since ITS applications imply strict packet delay constraints, a dependable connectivity is crucial. Accurate V2V radio channel models are therefore required, as channel statistics and dynamics ultimately define the reliability and robustness of vehicular communication systems.

In the past, propagation channel models for cellular systems have largely relied on the wide-sense stationarity (WSS) assumption [3]. The WSS assumption allows for a simplified statistical description of channels and forms the basis of many designs of wireless transceivers. However, owing to the rapidly changing environment when both link ends move, vehicular radio channels have been found to be non-stationary, i.e. the channel statistics can only be approximated as constant over a finite region in time or space. A visual inspection of the measured time-varying power delay profile (PDP) in, e.g., [4] and [5], validates the non-WSS of V2V channels. It was further observed that the interactions between strong clustered multipath components (clusters) and the line-of-sight (LOS) path change with time, including the splitting of clusters [6]. This must be accounted for, as [7] has pointed out that the WSS assumption in V2V channels could lead to (erroneous) optimistic bit-error-ratio (BER) simulation results in both single- and multi-carrier systems.

A process is considered to be WSS when its first and second order statistical moments are independent of absolute time. Several channel models have been proposed to represent the non-WSS of channels, see [8]–[10] and references therein. Whereas these theoretical frameworks are useful for non-WSS channel simulation, they hardly provide a measure to evaluate the quasi-stationarity region.

Meanwhile, to statistically characterize the radio channels, a local region of quasi-stationarity is needed in advance so that the small-scale fading parameters can be rigorously evaluated and the channel modeling becomes physically meaningful. Since communication algorithms often rely on knowledge of second order statistics of the channel, it is important to measure the size of local quasi-stationarity regions. Note that, in this paper, we use the term *quasi-stationarity* regions [11]–[13] not in its mathematical-statistical meaning but to express that the statistics of the channel are similar enough compared to the statistics of the neighboring channel such that the statistics can be approximately considered to be stationary. To substantiate the notion of "*similar enough*", appropriate measures of the similarity between channel statistics (i.e., for how long they can be considered to remain more or less constant) are required [14].

Part of the work is presented in the 35th Progress in Electromagnetics Research Symposium [1].

This work was supported by the Key Grant Project of Chinese Ministry of Education (No.313006), the National Natural Science Foundation of China under Grant 61222105 and U1334202, the National 863 Project under Grant 2014AA01A706, the Key Project of the State Key Lab of Rail Traffic Control and Safety under Grant RCS2012ZT013, the Fundamental Research Funds for the Central Universities under Grant 2014JBZ021, and the State Key Laboratory of Rail Traffic Control and Safety under Grant RCS2014ZZ03 and RCS2014ZT32.

R. He, Z. Zhong, and B. Ai* (correspondence author) are with the State Key Laboratory of Rail Traffic Control and Safety, Beijing Jiaotong University, Beijing 100044, China (e-mail: ruisi.he@bjtu.edu.cn, zhdzhong@bjtu.edu.cn, boai@bjtu.edu.cn).

O. Renaudin is with the Department of Electrical and Engineering, University of Southern California, Los Angeles, USA (e-mail: renaudin@usc.edu).

V.-M. Kolmonen is with Nokia Technologies, Finland (e-mail: velimatti.kolmonen@iki.fi).

K. Haneda is with the Department of Radio Science and Engineering, Aalto University, Aalto 00076, Finland (e-mail: katsuyuki.haneda@aalto.fi).

C. Oestges is with the Institute for Information and Communication Technologies, Electronics and Applied Mathematics, Université Catholique de Louvain, 1348 Louvain-la-Neuve, Belgium (e-mail: claude.oestges@uclouvain.be).

This article has been accepted for publication in a future issue of this journal, but has not been fully edited. Content may change prior to final publication. Citation information: DOI 10.1109/TAP.2015.2402291, IEEE Transactions on Antennas and Propagation

A. Related Work

Note that direct statistical tests for WSS of a random process exist, see [15]–[21] and references therein. However, a method characterizing the degree of non-WSS of doubly underspread random processes [8] is required since the wireless channel is inherently non-WSS [22], [23]. Several metrics have been proposed to measure the similarity between channel statistics, i.e., these metrics can be used to measure the size of quasi-stationarity region. We summarize some typical metrics as follows:

- Correlation matrix distance (CMD) [24]–[26], which is a measure to evaluate whether the changes in the spatial structure of the channel, was proposed to characterize the WSS of MIMO channels. In [13], [14], [27]–[29], the CMD was employed to characterize the non-WSS of vehicular MIMO channels.
- Spectral divergence (SD) [30], which measures the distance between strictly positive, non-normalized spectral densities, and can be applied to the PDPs [31] and the local scattering functions [8] measured at different times. In [32], the SD was used to analyze the non-WSS of vehicular channels, and in [33], the complexity of SD was investigated based on V2V measurements.
- Shadow fading correlation [34], which is a more traditional measure of the changes in channel statistics, and is so far not considered for V2V channels. Shadowing represents the variability of the received power around its expected value. The spatial autocorrelation function of shadowing is a measure of how fast the local shadowing evolves as the two mobile terminals (i.e., V2V) move along a certain route: the decorrelation distance of shadowing dictates how rapidly the environment changes, and can thus be considered as an equivalent quasi-stationarity distance.
- Other metrics: In [11], the local region of quasi-stationarity is defined based on the correlation between consecutive PDPs, which is not applicable to MIMO channels. In [13], an algorithm-specific approach from a system perspective is proposed and compared with the CMD, and the impact of polarization configuration of MIMO array is discussed. In [35], a modified mean square error metric is proposed and is found to have a similar behavior to CMD. In [36], it is suggested to identify the intervals of WSS by analyzing changes in the wavenumber spectrum estimated at different locations. In [37], the intervals of WSS is identified by comparing the delay power spectral density estimated at different time instances.

B. Discussion

In this paper, we make an important distinction between quasi-stationarity on *propagation level* and quasi-stationarity on *system level*. The former reflects the non-WSS characteristics of the *physical* propagation channel, as determined by the dynamic multipath components (MPCs) and is independent of the system configuration [1]. The latter is further affected by the system configuration (more specifically: bandwidth, which determines the MPC delay resolution, and antenna array, which determines the MPC angular resolution), and reflects the non-WSS characteristics that the system can "see". For a system with infinite bandwidth and perfect angular resolution, the quasi-stationarity on propagation level is naturally the same as the system-level quasi-stationarity. However, the estimated degree of non-stationarity reduces when the bandwidth and array size become limited. In such sense, the impacts of antenna array and bandwidth should be carefully analyzed.

C. Motivation

Summarizing, the existing works have several limitations. In particular, a comparison of the measurement-based WSS evaluations from the three above most popular metrics (CMD, SD, and shadowing correlation) is currently lacking. It is still unclear whether the three metrics lead to similar evaluations or not. As a corollary, how to select a suitable metric for non-WSS characterization is an open question. Compared to previous works, the main contributions of this paper are thus as follows:

- We characterize the non-WSS of V2V channels with recent MIMO V2V measurements and address the impacts of some factors (LOS / non-LOS (NLOS), speed of cars, number of antennas, environments) on the evaluation of non-WSS.
- A shadowing-correlation based equivalent quasi-stationarity distance is introduced to characterize the non-WSS of V2V channels.
- The size of the estimated quasi-stationarity regions using three metrics are carefully compared with each other and recommendations on how to select the most suitable metric (in the sense of better predicting the propagation-level quasi-stationarity) are suggested.

D. Outline

The remainder of the paper is organized as follows. Section II shows the measurement system and campaign. Section III introduces the three metrics to investigate the non-WSS of channels. Section IV presents the characterizations of non-WSS and compares the results in different scenarios. Finally, Section V concludes the paper.

II. Measurement Setup

A. Measurement system

The Aalto channel sounder [38], which is based on the switched-array principle, was used in the measurements. The measurements were conducted at 5.3 GHz, with a bandwidth of 60 MHz. Since propagation conditions do not vary significantly over 10-20% relative bandwidth, the 5.3 GHz band is deemed close enough to the 5.9 GHz band dedicated to V2V communications such that no significant differences in

[1] In that sense, it could be applied to any system configuration, in the same way as a wideband channel model could be reduced to a narrowband model (the opposite is not true).

This article has been accepted for publication in a future issue of this journal, but has not been fully edited. Content may change prior to final publication. Citation information: DOI 10.1109/TAP.2015.2402291, IEEE Transactions on Antennas and Propagation

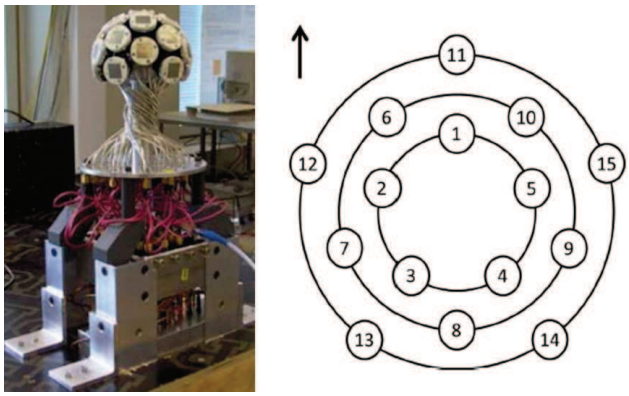

Fig. 1. Semi-spherical antenna array at the Rx side. Left: photo of the Rx semi-spherical antenna array. Right: Antenna element numbering. The arrow indicates the reference direction of the array.

TABLE I
SYSTEM PARAMETERS

Parameter	Value
Center frequency	5.3 GHz
Transmit power	36 dBm
Measurement bandwidth	60 MHz
Snapshot interval	15 ms

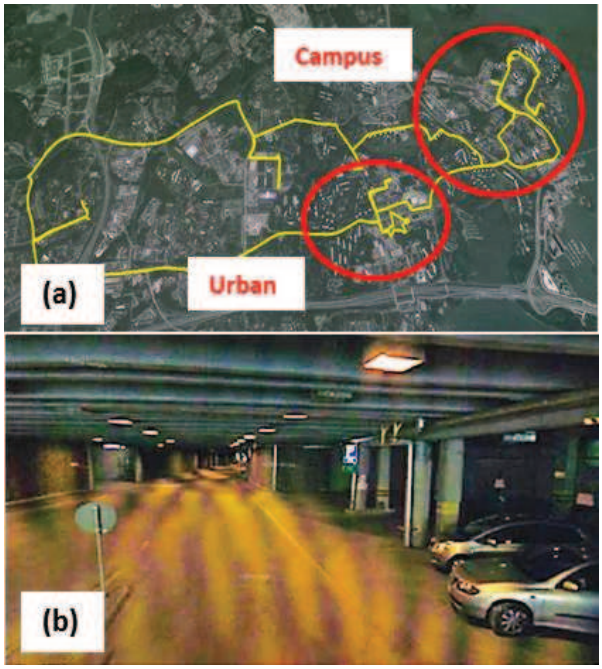

Fig. 2. (a) Top view of measurement routes. The urban and campus areas are marked, and the remaining routes are in suburban area. (b) Underground (tunnel-like) parking scenario, which is located in the urban area.

the channel propagation properties are to be expected. The snapshot time (i.e., the time required to measure all antenna pair channels) was set at 1.632 ms, whereas the snapshot repetition rate was set at 66.7 Hz[2]. The transmit power was 36 dBm. The main system parameters are summarized in Table I.

A dual-polarized semi-spherical antenna array was used at the receive (Rx) side. The antenna arrays consist of 15 dual-polarized (horizontal and vertical) elements (i.e. 30 feeds), which are arranged in a spherical geometry, as shown in Fig. 1. The diagonal of the Rx antenna is $\lambda/2$ in length, where λ is wavelength, and the diameter of the antenna ground plane is 3 cm. The radius of the sphere is 0.8λ, which corresponds to a neighboring element distance of $\lambda/2$. The radiation pattern of each Rx element is directive (according to its position in the antenna array), but the overall one can be considered as omnidirectional (since elements are oriented in all directions). More details of the Rx antenna array can be found in [38]. A Uniform Linear Array (ULA) with 4 vertically polarized omnidirectional antenna elements (with an interval of $\lambda/2$) was used at the transmit (Tx) side, as detailed in [1], [39].

Both Tx and Rx antenna arrays were mounted on wooden platforms installed on the roof of two compact cars, with a height of 50 cm above the roof. Note that the Tx car was always traveling ahead of the Rx car, and the reference direction of the Rx antenna array (as shown in Fig. 1) was always pointing towards the front of the Rx car (i.e. in the direction of motion of the Rx car). As the Rx antennas receive the signals from different directions due to the layout of the semi-spherical array, we cluster the antenna elements at Rx by defining the "front" elements with numbers 1, 2, 5, 6, 10, 11, 12, and 15 in Fig. 1, and the "back" elements with the remaining numbers. This grouping enables us to evaluate the impacts of different array configurations on the channel WSS[3]. Therefore, the MIMO channel matrix is $N_{\mathrm{Rx}} \times N_{\mathrm{Tx}} = 16 \times 4$ for "Tx-Rx front" side and $N_{\mathrm{Rx}} \times N_{\mathrm{Tx}} = 14 \times 4$ for "Tx-Rx back" side, respectively. Elevation differences of antennas are not considered in the grouping because the elevation difference is only tens of centimeters, and the LOS condition plays a huger role in our work.

B. Environments and Scenarios

The measurement campaign was conducted in four different environments in Finland: on a campus (Otaniemi), as well as in suburban (Tapiola), urban (Tapiola city center), and underground parking (Tapiola city center) areas. Fig. 2(a) shows the top view of the measurement routes. The campus and suburban areas mostly consist of small detached houses, parking lots, and an average tree density of roughly 5 m high. There are large sidewalks and road signs sparsely distributed

[2]The snapshot repetition rate of 66.7 Hz limits the maximum resolvable Doppler shift to 33.35 Hz, which is smaller than the maximum Doppler shift that can be expected in typical vehicular environments. Therefore, the temporal behavior of the multipath components stemming from the discrete scatterers will be undersampled and the Doppler information can not be reliably estimated [39]. However, since we do not analyze the Doppler behavior and we average out the small-scale fading when using the above metrics, the snapshot repetition rate does not affect our accuracy of analysis.

[3]An alternative grouping is to distinguish the "front, back, left, and right" sides of Rx antenna elements. The "left" and "right" cases correspond to the scatterer contributions from the roadsides. However, for our semi-spherical antenna array at Rx (as shown in Fig. 1), the "left" and "right" antenna elements can still receive strong (pure) LOS component, the differences of underlying propagation mechanisms between "front" and "left/right" cases are minor. Therefore, considering the additional complexity and the relatively small benefits of introducing the "left/right" cases, we only distinguish the "front" and "back" cases in this paper.

This article has been accepted for publication in a future issue of this journal, but has not been fully edited. Content may change prior to final publication. Citation information: DOI 10.1109/TAP.2015.2402291, IEEE Transactions on Antennas and Propagation

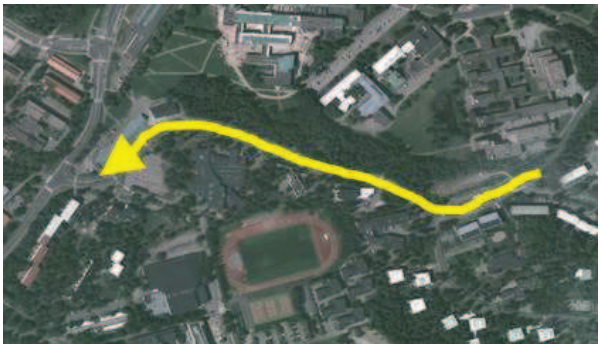

Fig. 3. Top view of the example measurement route in S1 scenario.

on both sides of the two-lane road. As the campus and suburban areas are similar to each other, we thus call them suburban in the following analysis. The city center of Tapiola consists of three to four-storey buildings on both sides of two-lane streets, occasional large open areas covered with vegetation and numerous road signs. The underground (tunnel-like) parking is under the ground of Tapiola city center, which is a rich scattering environment due to the tunnel-like structure. A photo of the underground parking is shown in Fig. 2(b). In total, we conducted the measurements along 22 different routes, with around 2000-7000 snapshots on each route.

The measurements were made with cars driving in the same direction (convoy), mainly under LOS conditions, although occasional obstruction of the LOS path did occur owing to different traffic conditions. We also conducted the measurements under NLOS conditions where the LOS between Tx and Rx was always blocked by other vehicles, e.g., trucks, and distinguish this case from other measurement runs.

The inter-vehicle distance varied between 10 and 500 m, depending on the traffic conditions, which ranged from no traffic at all (in the underground parking area) to heavy (in the urban and the NLOS suburban areas). In most of the suburban measurements, the traffic was between light and medium[4].

To analyze the stationarity, we consider 3 factors: environment, LOS/NLOS condition and the speed of cars. Hence, we re-group our measurements into 5 scenarios:

- S1: suburban LOS scenario, with a speed of 5-15 km/h.
- S2: suburban NLOS scenario, with a speed of 5-15 km/h.
- S3: suburban LOS scenario, with a speed of 30-40 km/h.
- S4: urban LOS scenario, with a speed of 5-15 km/h.
- S5: underground parking LOS scenario, with a speed of 5-15 km/h.

The choice of speed is a compromise between the desire to improve resolution in the time domain (requiring lower speed), and the necessity to ensure short measurement time for data storage in our setup (which require higher speed), as detailed in [39]. In each scenario, we characterize the non-WSS of V2V channels using the metrics reported in the following section.

[4]Here, "light traffic" means almost no traffic at all (only very few vehicles passing during the measurements, e.g. around 5 during each measurement route, i.e., 5/minute); "medium traffic" corresponds to situations when you have a little more vehicles passing (e.g. around 10-20/minute); and "heavy traffic" corresponds to situations when you have more vehicles in the traffic (e.g. around 30-60/minute).

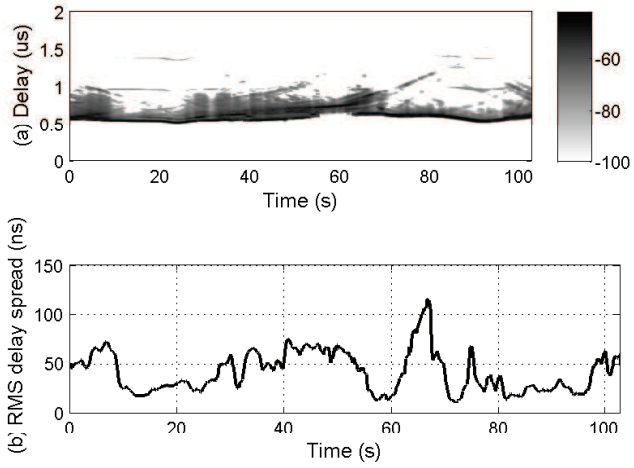

Fig. 4. Example measurements in S1 scenario. (a) APDPs. (b) RMS delay spread.

III. Measures of Channel Quasi-Stationarity

In this section, we describe the metrics used for estimating the size of the quasi-stationarity regions. For convenience, we use an example route in S1 scenario, whose view is shown in Fig. 3, and present the data processing using the measurements in this example route. The route is located on campus of Otaniemi. In the middle of the route there are heavy trees around; whereas for the beginning and end parts, there are small open areas. The traffic in the measurements was medium. The data post processing is presented and some typical channel parameters are discussed as follows using the example measurements .

A. Data Post Processing and Discussion

Our analysis is based on the measured impulse response $h(n, m, it_{\text{rep}}, p\tau_{\text{rep}})$ between the m-th Tx and n-th Rx antennas, where i is the time index, $t_{\text{rep}} = 15$ ms is the snapshot time interval, p is the delay bin index, and $\tau_{\text{rep}} = 8.33$ ns is the delay interval between two consecutive delay bins. From that, we define the instantaneous PDP as

$$P(n, m, it_{\text{rep}}, p\tau_{\text{rep}}) = |h(n, m, it_{\text{rep}}, p\tau_{\text{rep}})|^2, \quad (1)$$

where $|\cdot|$ denotes the absolute value. The instantaneous path gain for each Tx-Rx link is expressed as

$$P_G(n, m, it_{\text{rep}}) = \sum_{p=1}^{N_\tau} P(n, m, it_{\text{rep}}, p\tau_{\text{rep}}), \quad (2)$$

where $N_\tau = 510$ is the number of delay bins in each snapshot. Before characterizing the non-WSS channels, a window should be defined to remove the impact of small-scale fading, then the size of the quasi-stationarity region can be evaluated. This window has to be large enough to accurately estimate correlation matrices but also small enough to average over snapshots having the same (local) statistics. In this paper, we use a 40-wavelength window, which has been suggested for V2V scenarios, e.g., in [27], [28]. Later, it is found that

This article has been accepted for publication in a future issue of this journal, but has not been fully edited. Content may change prior to final publication. Citation information: DOI 10.1109/TAP.2015.2402291, IEEE Transactions on Antennas and Propagation

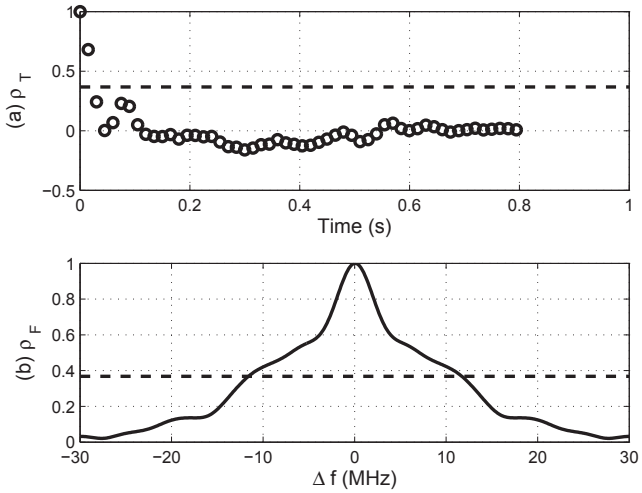

Fig. 5. (a) Example plot of the envelope autocovariance function in S1 scenario, together with the threshold of 1/e. (b) Example plot of the frequency correlation function in S1 scenario, together with the threshold of 1/e.

the estimated quasi-stationarity region has a larger size than the 40-wavelength window. This indicates that the estimation of the correlation matrices is performed over time intervals during which the channel statistics remain approximately constant (i.e. WSS). The averaged PDPs (APDPs) over the 40-wavelength window and all antenna elements for the example route are presented in Fig. 4(a), and the corresponding root-mean-square (RMS) delay spread [40] is plotted in Fig. 4(b). In the calculation of RMS delay spread, the paths with a power below the noise floor plus 6 dB have already been removed [41]. We can see that in APDPs there are two regions (10-25 s and 70-95 s, as marked in Fig. 4(a)) with a small number of scattering components after the LOS component. These two regions correspond to the open areas in the beginning and the end of the route, as in Fig. 3. For the other regions of APDPs, there are relatively rich scattering components after the LOS path, which are mostly caused by the surrounding heavy trees and traffics. For the two regions with few scattering components, the corresponding RMS delay spreads are very small with a mean value of 25.41 ns; while the mean value of the RMS delay spreads in other regions is 51.64 ns.

It is also necessary to have enough samples in the averaging window so that sufficient accuracy of the statistical estimation can be achieved [42], [43]. Therefore, we examine the auto-correlation of the small-scale fading and the coherence bandwidth of the measurements:

- The envelope autocovariance function ρ_{T} of the small-scale fading determines the correlation of received envelope as a function of change in receiver position [44]. After removing the mean value of $P_G(n,m,it_{\mathrm{rep}})$ within each 40-wavelength window, we get the small-scale fading envelope $SS(n,m,it_{\mathrm{rep}})$ for each Tx-Rx link, expressed as

$$SS(n,m,it_{\mathrm{rep}}) = \sqrt{\frac{P_G(n,m,it_{\mathrm{rep}})}{\sum_{k=i}^{i+W-1} P_G(n,m,kt_{\mathrm{rep}})}}\ , \qquad (3)$$

where W is the averaging interval. In all scenarios except S3, W was set to 54, which corresponds to a 40-wavelength window at 5.3 GHz with an average speed of 10 km/h, while for scenario S3 (with an average speed of 35 km/h), the 40-wavelength window corresponds to $W = 16$. Then, ρ_{T} can be calculated as

$$\rho_{\mathrm{T}}(n,m,\Delta i \cdot t_{\mathrm{rep}}) = \frac{E\left\{SS(n,m,it_{\mathrm{rep}}) \cdot SS(n,m,(i+\Delta i)t_{\mathrm{rep}})\right\}}{\sigma_{SS}}\ , \qquad (4)$$

where $E\{\cdot\}$ denotes the expected value of $\{\cdot\}$. σ_{SS} is the standard deviation of small-scale fading components. The envelope autocovariance function at each location is estimated, and a threshold of 1/e is used to determine the coherent time [40]. An example plot of the estimated ρ_{T} from the example route in Fig. 3 is shown in Fig. 5(a), where $t = 60$ s and $n = m = 1$. It is found that ρ_{T} drops below 1/e at the third sample. This phenomenon is observed in all the measurements, which means we have 27 independent samples over time/distance domain in the 40-wavelength window for all scenarios except S3; in S3, it corresponds to 8 independent samples.
- The coherence bandwidth B_{coh} is obtained from the frequency correlation function ρ_{F} [40], which is the Fourier transform of the APDPs, defined as in Eq. (5), where Δf is the frequency difference. B_{coh} is defined as the smallest value of Δf for which ρ_{F} drops below a threshold of 1/e [45]. ρ_{F} is estimated at each location for all measurements, and an example plot of the estimated ρ_{F} from the example route in Fig. 3 is shown in Fig. 5(b), where $B_{\mathrm{coh}} = 11.7$ MHz. It is found that over all the measurements, B_{coh} has a mean value of 10 MHz. This means at each location, we have around 6 independent samples over the 60 MHz bandwidth.

The above analysis shows that we have around $27 \times 6 = 162$ independent samples within the 40-wavelength window for all scenarios except S3; whereas in S3, the number of independent samples is around $8 \times 6 = 48$. These numbers of independent samples ensure an accurate analysis of the channel statistics[5]. In the following, the three metrics used to characterize the size of quasi-stationarity region are introduced.

B. Correlation Matrix Distance

The CMD is useful to evaluate whether the spatial structure of the channel, i.e., the angles of departure/arrival of paths, have changed in a significant way. The CMD between the two correlation matrices $\mathbf{R}(it_{\mathrm{rep}})$ and $\mathbf{R}(jt_{\mathrm{rep}})$ measured at times it_{rep} and jt_{rep} is defined by

$$d_{\mathrm{corr}}(i,j) = 1 - \frac{\mathrm{tr}\left\{\mathbf{R}(it_{\mathrm{rep}}) \cdot \mathbf{R}(jt_{\mathrm{rep}})\right\}}{\|\mathbf{R}(it_{\mathrm{rep}})\|_f \cdot \|\mathbf{R}(jt_{\mathrm{rep}})\|_f}, \qquad (6)$$

where i and j are the time indices. $\mathrm{tr}\{\cdot\}$ and $\|\cdot\|_f$ denotes the trace and Frobenius norm of a matrix. The CMD is zero if the correlation matrices are equal up to a scaling factor

[5]As a comparison, it has been confirmed in [42] that for Rayleigh channel the sufficient number of samples for estimating the local average power values is about 36, within 40-wavelength window.

This article has been accepted for publication in a future issue of this journal, but has not been fully edited. Content may change prior to final publication. Citation information: DOI 10.1109/TAP.2015.2402291, IEEE Transactions on Antennas and Propagation

$$\rho_{\mathrm{F}}(\Delta f, it_{\mathrm{rep}}) = \int_{-\infty}^{\infty} \frac{\sum_{n=1}^{N_{\mathrm{Rx}}} \sum_{m=1}^{N_{\mathrm{Tx}}} \sum_{k=i}^{i+W-1} P(n, m, it_{\mathrm{rep}}, p\tau_{\mathrm{rep}})}{N_{\mathrm{Rx}} N_{\mathrm{Tx}} W} \times \left(e^{-j2\pi\Delta f p\tau_{\mathrm{rep}}} \cdot \tau_{\mathrm{rep}}\right) dp \tag{5}$$

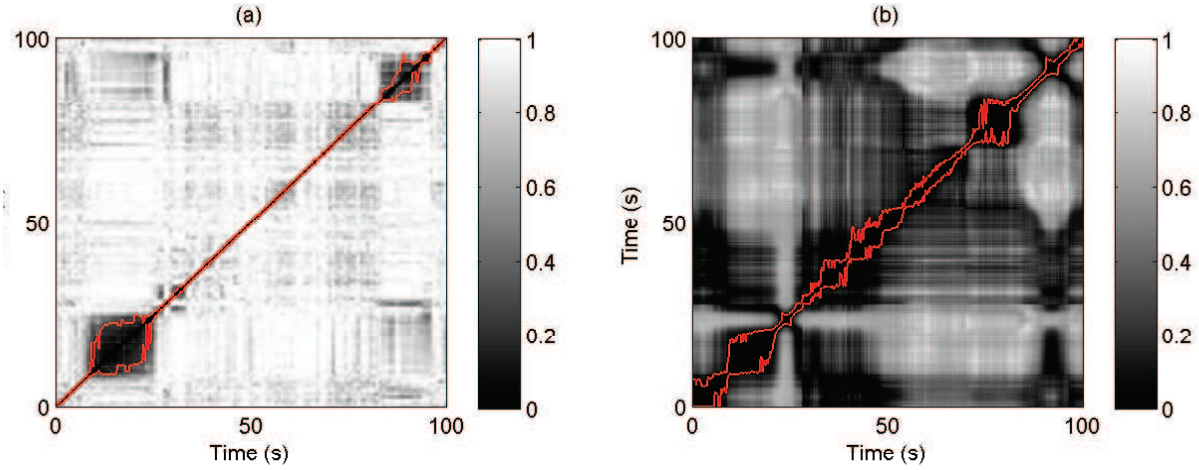

Fig. 6. Estimated CMD and SD for the example route in S1 scenario. (a) CMD, front case, using full channel correlation matrix. (b) SD, front case. The corresponding time-variant quasi-stationarity intervals are marked using red curves. The thresholds for CMD and SD are 0.2 and 0.05, respectively.

and one if they are completely uncorrelated. The narrowband complex MIMO channel matrices $\mathbf{H}(kt_{\mathrm{rep}})$ are obtained from the $N_{\mathrm{Rx}} \times N_{\mathrm{Tx}}$ measured impulse responses matrices $\mathbf{h}(kt_{\mathrm{rep}}, p\tau_{\mathrm{rep}})$ [40], as

$$\mathbf{H}(kt_{\mathrm{rep}}, \Delta f) = \sum_{p=1}^{N_\tau} \mathbf{h}(kt_{\mathrm{rep}}, p\tau_{\mathrm{rep}}) \cdot e^{-j2\pi\Delta f p\tau_{\mathrm{rep}}}. \tag{7}$$

Then, the CMD can be computed either at both Tx and Rx sides when using Tx and Rx correlation matrices respectively, or computed with full channel correlation matrix [25], which are defined as in Eq. (8), where B is measurement bandwidth, $(\cdot)^{\mathrm{T}}$ denotes transpose, $(\cdot)^*$ denotes conjugation, $(\cdot)^{\mathrm{H}}$ denotes hermitian transpose, and $\mathrm{vec}\,[\cdot]$ operator stacks a matrix into a vector columnwise.

Fig. 6(a) shows an example plot of the estimated CMD between arbitrary times of the example route. It is observed that there are generally two quasi-stationarity regions (i.e., the regions with small values of CMD) in CMD plots, corresponding to the regions of 10-25 s and 70-95 s. This means that the region with a large delay spread (as shown in Fig. 4) corresponds to a reduced quasi-stationarity of channels. This phenomenon is also observed in other measurements. Moreover, we note that the CMDs are different at Tx and Rx sides, where at Tx side the CMD shows a larger quasi-stationarity region than Rx side; while the CMD using the full channel correlation matrix has the smallest quasi-stationarity region. More detailed analysis of WSS is presented in the following section.

For CMD metric, time-variant quasi-stationarity time is defined as the maximum period over which the CMD remains below a certain threshold c_{th}, expressed as [39]

$$T(i) = (i'_{\max} - i'_{\min}) \cdot t_{\mathrm{rep}} \ , \tag{9}$$

where the time-variant minimum and maximum bounds of the quasi-stationarity intervals at time it_{rep} are

$$\begin{cases} i'_{\min} = \underset{0\le j\le i-1}{\arg\max}\, d_{\mathrm{corr}}(i,j) \ge c_{\mathrm{th}} \\ i'_{\max} = \underset{i+1\le j\le N_t-W}{\arg\min}\, d_{\mathrm{corr}}(i,j) \ge c_{\mathrm{th}} \end{cases}, \tag{10}$$

and $i = 0, 1, \cdots, N_t - W$. N_t is the total number of snapshots. Finally, the size of the quasi-stationarity region is the product of the quasi-stationarity time and average speed.

For CMD metric (also for SD metric), the estimation is significantly affected by the threshold c_{th}. To avoid the arbitrary selection of threshold, a visual inspection of the estimation and comparisons of the results with different thresholds are required [14]. The less restrictive the threshold is, the larger the quasi-stationarity region is. Therefore, in this paper, we propose a suitable threshold for V2V channels using following strategies:

- First, a heuristic c_{th} is defined as the maximum value of the thresholds where the estimation of quasi-stationarity region generally remains unchanged, i.e., a threshold larger than c_{th} will lead to a significantly increase of the estimated size of quasi-stationarity region. This heuristic definition is similar to [14]. We plot in Fig. 7(a) and (b) the time-varying quasi-stationarity distance for the example measurements using CMD metric. The results obtained with three different thresholds are plotted for comparison, where it is found that the results from thresholds 0.1 and 0.2 are close to each other, and the results of threshold 0.3 are much higher than others, especially at 10-25 s. 0.2 can thus be considered as a reasonable threshold here.
- Then, to further discuss the impact of threshold on the estimation of quasi-stationarity region size, we examine

This article has been accepted for publication in a future issue of this journal, but has not been fully edited. Content may change prior to final publication. Citation information: DOI 10.1109/TAP.2015.2402291, IEEE Transactions on Antennas and Propagation

$$\mathbf{R}_{\mathrm{Tx}}(it_{\mathrm{rep}}) = \frac{1}{B \cdot W} \sum_{\Delta f=-B/2}^{B/2} \sum_{k=i}^{i+W-1} \mathbf{H}(kt_{\mathrm{rep}}, \Delta f)^{\mathrm{T}} \mathbf{H}(kt_{\mathrm{rep}}, \Delta f)^{*}$$
$$\mathbf{R}_{\mathrm{Rx}}(it_{\mathrm{rep}}) = \frac{1}{B \cdot W} \sum_{\Delta f=-B/2}^{B/2} \sum_{k=i}^{i+W-1} \mathbf{H}(kt_{\mathrm{rep}}, \Delta f) \mathbf{H}(kt_{\mathrm{rep}}, \Delta f)^{\mathrm{H}} \tag{8}$$
$$\mathbf{R}_{\mathrm{Full}}(it_{\mathrm{rep}}) = \frac{1}{B \cdot W} \sum_{\Delta f=-B/2}^{B/2} \sum_{k=i}^{i+W-1} \mathrm{vec}\left[\mathbf{H}(kt_{\mathrm{rep}}, \Delta f)\right] \mathrm{vec}[\mathbf{H}(kt_{\mathrm{rep}}, \Delta f)]^{\mathrm{H}}$$

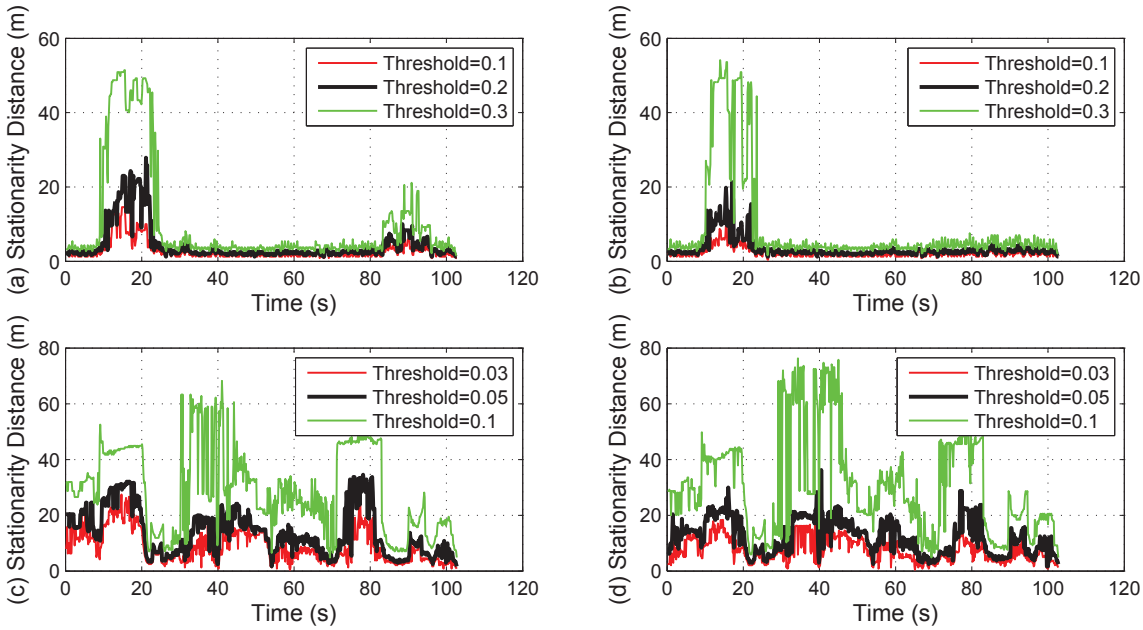

Fig. 7. Estimated time-varying quasi-stationarity distance for the example measurements in S1 scenario with different thresholds. (a) CMD, front case, using full channel correlation matrix. (b) CMD, back case, using full channel correlation matrix. (c) SD, front case. (d) SD, back case.

the variations of quasi-stationarity region size against threshold. Example plots of quasi-stationarity region vs threshold are shown in Fig. 8. It is not surprising that a lower threshold leads to a smaller quasi-stationarity region. We also note that in Fig. 8, 0.2 can be approximately considered as a inflection point of the CMD curve. Other measurements were examined by visual inspection and it is found that reasonable values of estimation can generally be obtained with the threshold of 0.2.

- Finally, we compare the thresholds of CMD in open literature. In [24]–[28], [39], a threshold of 0.2 is suggested. In [12], [29], a threshold of 0.1 is suggested. In [13], [14], different thresholds are discussed. Generally, 0.2 is more common for CMD metric. In Fig. 6 we plot the corresponding time-variant quasi-stationarity intervals for comparison.

Therefore, in this paper, the threshold for CMD is set at 0.2.

C. Spectral Divergence

The SD measures the distance between spectral densities. A smaller SD corresponds to a stronger correlation between the two spectral densities. We apply SD to the PDPs in this paper to have a unified measure as in CMD. It is defined as [31]

$$\gamma(i,j) = \log_e \left(\frac{1}{N_\tau^2} \cdot \sum_{p=1}^{N_\tau} \frac{\overline{P}(it_{\mathrm{rep}}, p\tau_{\mathrm{rep}})}{\overline{P}(jt_{\mathrm{rep}}, p\tau_{\mathrm{rep}})} \cdot \sum_{p=1}^{N_\tau} \frac{\overline{P}(jt_{\mathrm{rep}}, p\tau_{\mathrm{rep}})}{\overline{P}(it_{\mathrm{rep}}, p\tau_{\mathrm{rep}})} \right), \tag{11}$$

where the instantaneous PDP is averaged over Tx and Rx elements within each subset (the "front" and "back" cases), as

$$\overline{P}(it_{\mathrm{rep}}, p\tau_{\mathrm{rep}}) = \frac{1}{N_{\mathrm{Rx}} N_{\mathrm{Tx}}} \sum_{n=1}^{N_{\mathrm{Rx}}} \sum_{m=1}^{N_{\mathrm{Tx}}} |h(n, m, it_{\mathrm{rep}}, p\tau_{\mathrm{rep}})|^2. \tag{12}$$

We normalize (11) to the maximum value at each location so that the normalized SD is bounded between 0 and 1, which makes it possible to define a unified threshold. Fig. 6(b) shows a plot of the normalized SD between arbitrary times for the measurements of the example route in Fig. 3. We can also observe the two quasi-stationarity regions around 10-25 s and 70-95 s from the estimated SD, which is similar to the results of CMD. It is also noted that the normalized SD is generally smaller than CMD, therefore, a smaller threshold should be applied to SD metric (as discussed later).

The time-variant quasi-stationarity time for SD is also defined as the maximum period over which the SD remains below a certain threshold, as in (9) and (10), and we determine

This article has been accepted for publication in a future issue of this journal, but has not been fully edited. Content may change prior to final publication. Citation information: DOI 10.1109/TAP.2015.2402291, IEEE Transactions on Antennas and Propagation

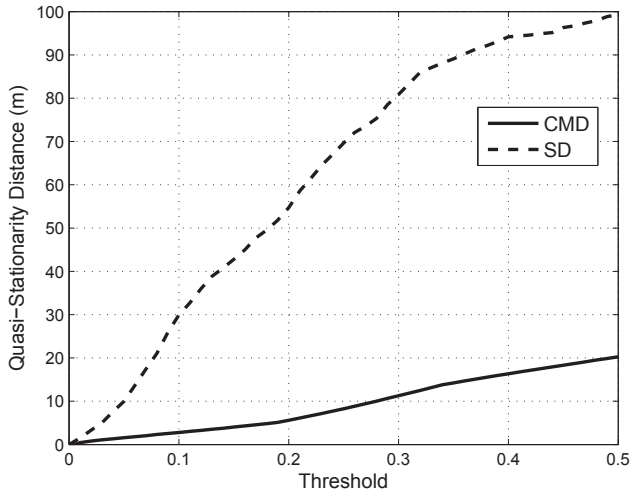

Fig. 8. Mean value of the estimated time-varying quasi-stationarity distance for the example measurements in S1 scenario with different thresholds: CMD - front case, using full channel correlation matrix; SD - front case.

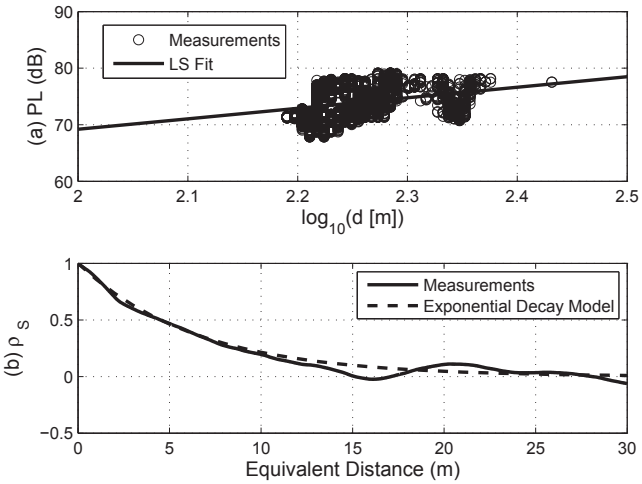

Fig. 9. Example plots of the "front case" measurements for the route in Fig. 3. (a) Path loss. (b) Auto-correlation coefficient of shadow fading, together with the exponential decay model.

the threshold of SD using the same principle to CMD. Fig. 7(c) and (d) show the time-varying quasi-stationarity distance for the example measurements using SD metric, with three different thresholds. It is found that the results from thresholds 0.03 and 0.05 are close to each other, and they are also close to the results of CMD: they all show a large quasi-stationarity region for 10-25 s and 70-95 s regions, which correspond to the regions with large delay spread as in Fig. 4. However, for the results of SD with a threshold of 0.1, a large quasi-stationarity region is observed at 30-70 s, which is different to the results in other cases. Therefore, a threshold of 0.05 should be used here. In Fig. 8, we plot the SD curve of quasi-stationarity region vs threshold, where the quasi-stationarity distance increases with threshold. We note that the slope of SD curve is larger than the CMD curve. This means that the CMD and SD metrics have different sensitivities. The SD metric is more sensitive to the variation of threshold. Similarly to the CMD metric, all other measurements of SD were examined by visual inspection and it is found that reasonable values of estimation can generally be obtained with the threshold of 0.05. In Fig. 6 we plot the corresponding time-variant quasi-stationarity intervals for comparison, which indicates reasonable performance. Therefore, in this paper, the threshold for SD is set at 0.05. Note that in open literature, few thresholds are suggested for the SD metric, this is because the SD without normalization is an unbounded metric [14].

D. Shadowing Correlation

As the changes of channel statistics affect the auto-correlation property of shadow fading, the auto-correlation coefficient also describes the WSS of channels. The auto-correlation coefficient of shadow fading is expressed as

$$\rho_S(\Delta k t_{\rm rep}) = \frac{E\left\{X(kt_{\rm rep})X(kt_{\rm rep}+\Delta kt_{\rm rep})\right\}}{\sigma}\ , \quad (13)$$

where $X(kt_{\rm rep})$ is the shadow fading component measured at time index k, and σ is the standard deviation of shadow fading. The procedure for obtaining $X(kt_{\rm rep})$ is as follows:

- We first average the instantaneous path gain in (2) over Tx/Rx (within each subset of "front" and "back" cases) and the 40-wavelength window, as follows

$$\overline{P_G}(kt_{\rm rep}) = \frac{1}{W}\sum_{i=k}^{k+W-1}\left(\frac{\sum_{n=1}^{N_{\rm Rx}}\sum_{m=1}^{N_{\rm Tx}}\sum_{p=1}^{N_\tau}|h(n,m,it_{\rm rep},p\tau_{\rm rep})|^2}{N_{\rm Rx}N_{\rm Tx}N_\tau}\right). \quad (14)$$

  This removes the small-scale fading.
- Then we use the delay $\tau_{\rm LOS}(k)$ of the LOS component in $\overline{P}(kt_{\rm rep}, p\tau_{\rm rep})$ to estimate the corresponding Tx-Rx distance d_k for $\overline{P_G}(kt_{\rm rep})$, as

$$d_k = \tau_{\rm LOS}(k)\cdot c\ , \quad (15)$$

  where c is the speed of light. $\overline{P_G}(kt_{\rm rep})$ can thus be re-written as $\overline{P_G}(kt_{\rm rep}, d_k)$. Here only the LOS delay bins in the "front" elements' $\overline{P}(kt_{\rm rep}, p\tau_{\rm rep})$ were used to estimate d_k, as Tx car was always moving ahead of Rx car. After plotting the measured $\overline{P_G}(kt_{\rm rep}, d_k)$ versus the estimated d_k in logarithmic scale, the log-distance path gain model $\overline{P_{G,\rm LS}}(kt_{\rm rep}, d_k)$ can be obtained by using a least-square (LS) fit. Fig. 9(a) shows an example plot of the distance-dependent path loss (which is the inverse of the path gain) model fit, where the path loss exponent is 1.86.
- We remove $\overline{P_{G,\rm LS}}(kt_{\rm rep}, d_k)$ out of the corresponding $\overline{P_G}(kt_{\rm rep}, d_k)$ to get shadow fading component $X(kt_{\rm rep}, d_k)$ by

$$X(kt_{\rm rep}, d_k) = \overline{P_{G,\rm LS}}(kt_{\rm rep}, d_k) - \overline{P_G}(kt_{\rm rep}, d_k). \quad (16)$$

  We drop the distance information d_k in $X(kt_{\rm rep}, d_k)$ so that the shadow fading component changes back to the time-series data $X(kt_{\rm rep})$. Finally, the auto-correlation

This article has been accepted for publication in a future issue of this journal, but has not been fully edited. Content may change prior to final publication. Citation information: DOI 10.1109/TAP.2015.2402291, IEEE Transactions on Antennas and Propagation

coefficient of shadow fading can be calculated by using (13).

The decorrelation time, which depends on the scenario, is defined to be the time at which the auto-correlation coefficient drops to $1/e$. By multiplying it by the average speed, we obtain the decorrelation distance, which is considered as the shadowing-based equivalent quasi-stationarity distance. Fig. 9(b) shows the the auto-correlation coefficient for the route in Fig. 3 as an example, where the equivalent distance is the product of the average speed and $\Delta k t_{\mathrm{rep}}$. The classical exponential decay model [34] is plotted for comparison, which is found to fit the measurements very well. The equivalent quasi-stationarity distance in Fig. 9(b) is 6.50 m.

Note that this approach is only valid when we have LOS in the measurements[6]. As we do not have GPS information, we cannot remove the distance-dependent path gain for NLOS conditions, and we thus do not analyze the shadow fading for NLOS cases.

IV. Results

As mentioned, we estimate the equivalent quasi-stationarity distance (i.e., the size of quasi-stationarity region) as the product of the quasi-stationarity time and average speed. The CDFs of the equivalent quasi-stationarity distance are plotted in Fig. 10-14, using the above three measures. Note that we use different scalings on the x-axis for clarity. The estimated size of quasi-stationarity region is generally close to the results in [13], [14]. Compared with [27], our estimated quasi-stationarity region has a smaller size. We conjecture that this is because there was less traffic in the measurements of [27]. We also summarize the estimated mean value of the quasi-stationarity distance using different metrics in Table II. Several observations in Table II are worth noting and thus discussed as follows.

A. Tx and Rx Sides

The quasi-stationarity distances (estimated from CMD) at Tx and Rx sides largely differ. From Fig. 10-11 and Fig. 13-14, we can see that the CMD quasi-stationarity distance at Tx side is generally 10-50 m larger than at Rx side. In Fig. 12, the CMD quasi-stationarity distance at Tx side is sometimes even 100 m larger than at Rx side. This is different from the observations in [27], which suggested that the CMDs at Tx and Rx sides are very similar to each other. The reason for this apparent discrepancy is caused by the smaller Tx array size in our measurement, which results in a "worse angular resolution" and thus yields a larger quasi-stationarity region (in [27], the antenna arrays at Tx and Rx were both semi-spherical, with the same size).

Another observation is the CMD quasi-stationarity distances estimated using the full correlation matrix are slightly smaller than the results estimated at Rx side, which is similar to the results in [13]. This is because the full correlation matrix includes richer information of the channel spatial structure and thus improves the angular resolution. However, this prevents comparison and analysis of the estimated sizes of the quasi-stationarity region at both sides of Tx and Rx.

B. Front and Back Cases

From the CMD metric we find that in S1, S4, and S5 scenarios, the "front" case generally has a larger quasi-stationarity region than the "back" case. This is because the "front" array has a strong (LOS) component that dominates the radio wave propagation. Since it is relatively stable over time, we thus have long quasi-stationarity distance. While for the "back" case, the broadside of most antenna elements points towards opposite direction to the Tx, and there is no LOS so that weaker components (e.g., due to scatterers on the roadsides) have more importance in the radio wave propagation. Since these components are likely to appear/disappear rapidly (or their corresponding direction-of-arrival/direction-of-departure change) on small time scales, the structure of the MIMO channel will change faster than in the "front" case. In S2 scenario, the CMD quasi-stationarity of the "front" case is similar to the "back" case. This is because when the LOS is entirely blocked (i.e., NLOS), the received rays come from different directions due to the dynamic scatterers in the V2V environments, and whether the elements are in the front or back does not have a strong impact on the directions of the received rays anymore. In S3 scenario, it is found that the CMD "front" case has a smaller quasi-stationarity region than the "back" case. It is conjectured that this phenomenon is caused by the occasional distributions of the scatterers in S3 - there were more moving cars in the front side in the measurements. The LOS component is also in that case less dominant than in other scenarios, so that it yields shorter quasi-stationarity distance. However, we only have one measurement dataset in S3, so that further measurements are required to investigate the high-speed scenarios.

From SD and shadowing metrics, it is found that the "front" and "back" cases yield predictably similar results[7]. This is because the SD and shadowing correlation take only into account the power variations over time (and not the direction-of-arrival/direction-of-departure of the scatterer contributions, as the CMD does). Hence, if the power of the LOS and of the roadside components vary both similarly over time, then same SD and shadowing correlation can be obtained. On the other hand, the direction-of-arrival/direction-of-departure of the LOS component are more or less constant over time (as long as the relative orientation of the Tx and Rx vehicles doesn't change), while it is obviously not the case for the roadside scatterers. Hence, the CMD for the "front" case will lead to larger quasi-stationarity region than for the "back" case.

C. LOS and NLOS

From the comparison between S1 and S2, we can see that NLOS generally leads to a smaller quasi-stationarity region. This is not surprising since the NLOS channel is more sensible

[6]In our LOS measurements, only occasional obstruction of the LOS path occurred, so that this affects negligibly the accuracy of the estimated distance-dependent path gain model.

[7]Note that in S3 scenario there is huge difference between "front" and "back" cases for the shadowing-based metric. Again, this is probably caused by the reduced number of samples in dataset.

This article has been accepted for publication in a future issue of this journal, but has not been fully edited. Content may change prior to final publication. Citation information: DOI 10.1109/TAP.2015.2402291, IEEE Transactions on Antennas and Propagation

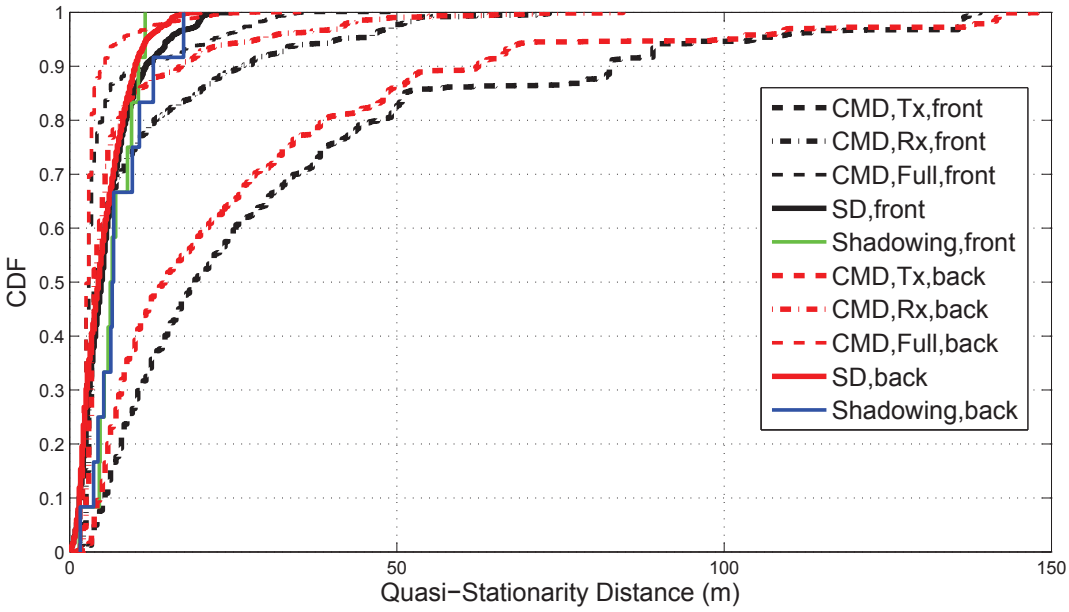

Fig. 10. Quasi-stationarity distance in S1 scenario.

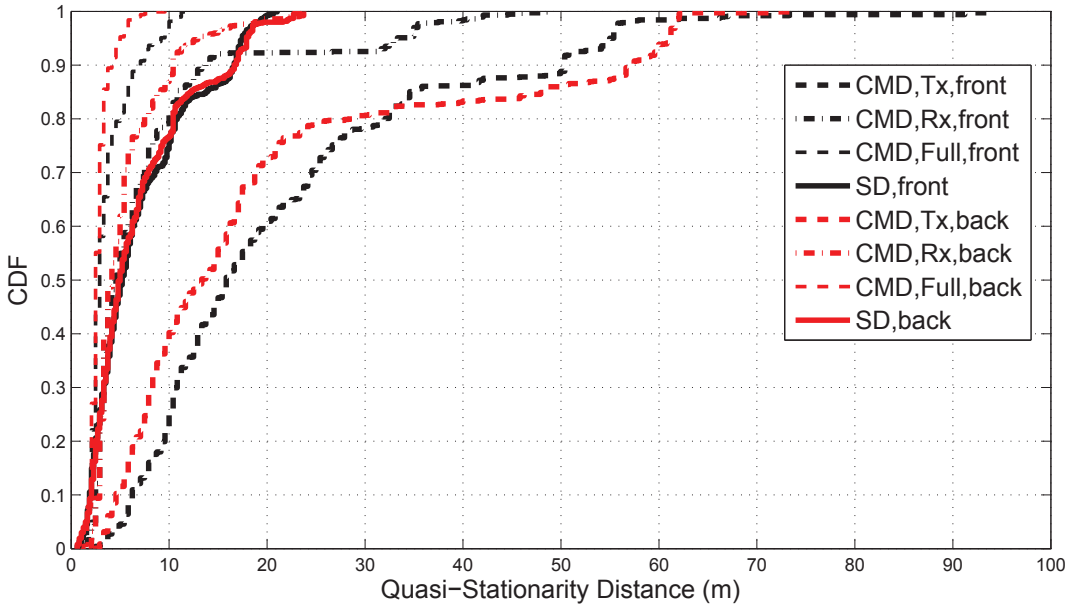

Fig. 11. Quasi-stationarity distance in S2 scenario.

to the impact roadside scatterers (either static or dynamic), as there is in that case no dominant component (e.g., the LOS one). While the LOS case always has a dominant LOS component.

D. Speed

It is found that S3 has the largest quasi-stationarity region. This is because in S3 the measurement cars have a speed closer to other cars on the road. Therefore, the reflection and scattering components from other cars generally have smaller dynamic changes over time, and the quasi-stationarity distance increases.

E. Environment

The underground parking scenario generally exhibits the smallest quasi-stationarity region, as it has rich scattering owing to multiple reflections and wave-guiding propagation effects (walls, ceilings, other vehicles, metallic structures as ventilation systems, etc.). The quasi-stationarity region in urban areas is smaller than in suburban areas, due to more scatterers in the former.

This article has been accepted for publication in a future issue of this journal, but has not been fully edited. Content may change prior to final publication. Citation information: DOI 10.1109/TAP.2015.2402291, IEEE Transactions on Antennas and Propagation

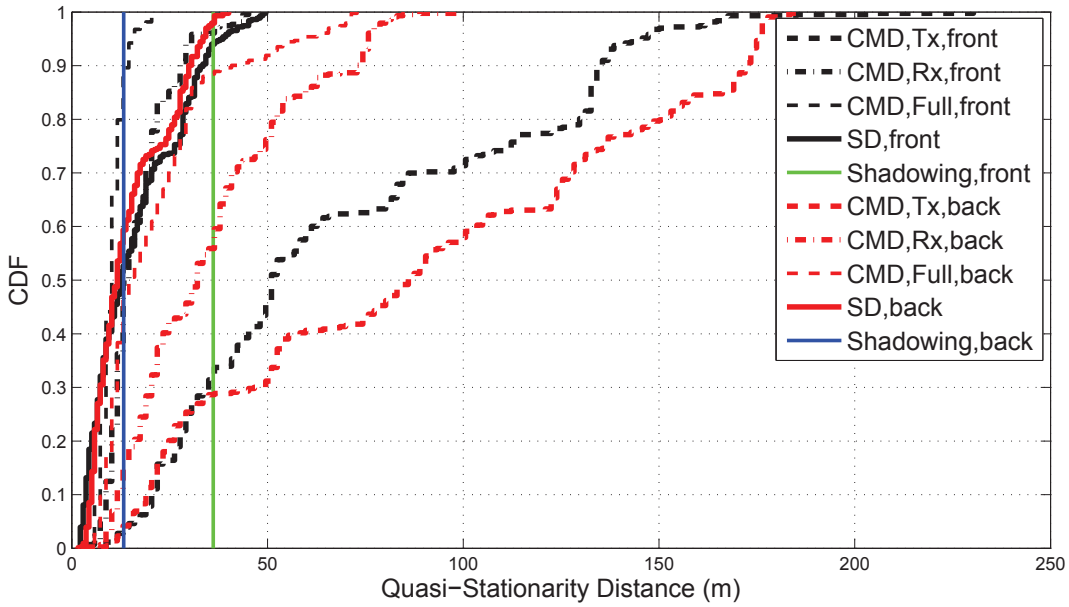

Fig. 12. Quasi-stationarity distance in S3 scenario. The step CDF curves of the results of shadowing are caused by the reduced dataset.

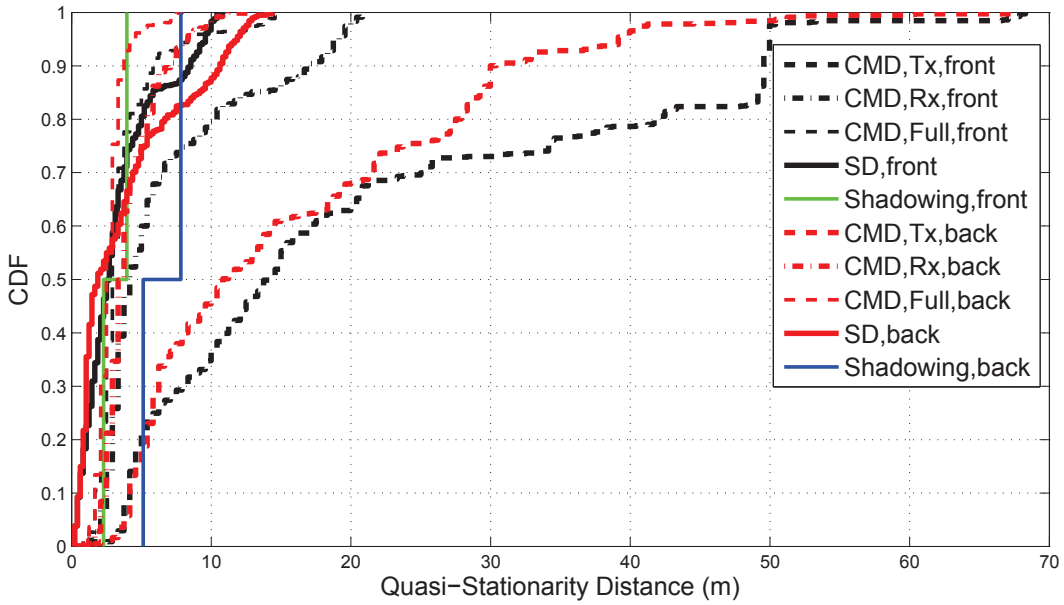

Fig. 13. Quasi-stationarity distance in S4 scenario.

F. Array Aperture

As pointed out before, the Rx array offers a better angular resolution due to a larger size of the array. However, the angular resolution is determined by the electrical aperture size of array, regardless of the number of antenna elements in it. Therefore, we examine the impact of the electrical array aperture on the quasi-stationarity estimation[8]. We use all the elements of Rx and re-group the elements at Tx side with three cases to get three new channel matrices: (i) Tx elements 1 and 2; (ii) Tx elements 1 and 4; and (iii) Tx elements 1, 2, 3, and 4. Then we estimate the quasi-stationarity distance with CMD using the above three channel matrices. Fig. 15 shows the estimated quasi-stationarity distance of the three cases above, using the measurements of the route in Fig. 2(c) as an example. It is found that case (i) has a larger quasi-stationarity distance than case (ii). This phenomenon follows the physical insight of beamforming resolution: for a ULA comprising M sensors, with inter-element spacing equal to Δd, the direction-of-arrival resolution $\Delta\theta$ of beamforming is

[8]We only do it using CMD metric because SD and shadowing metrics are independent from the array size.

This article has been accepted for publication in a future issue of this journal, but has not been fully edited. Content may change prior to final publication. Citation information: DOI 10.1109/TAP.2015.2402291, IEEE Transactions on Antennas and Propagation

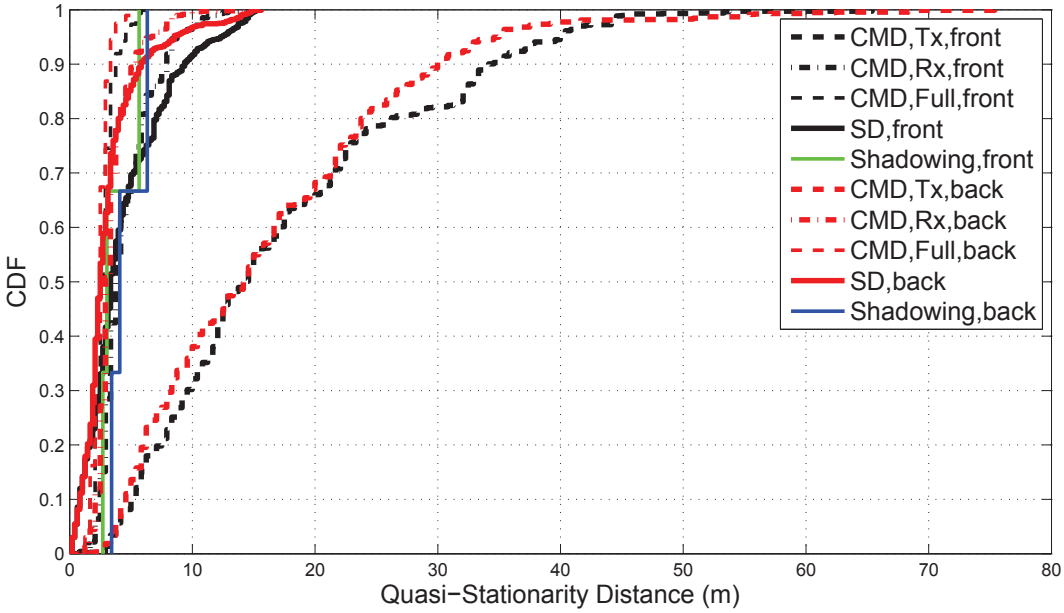

Fig. 14. Quasi-stationarity distance in S5 scenario.

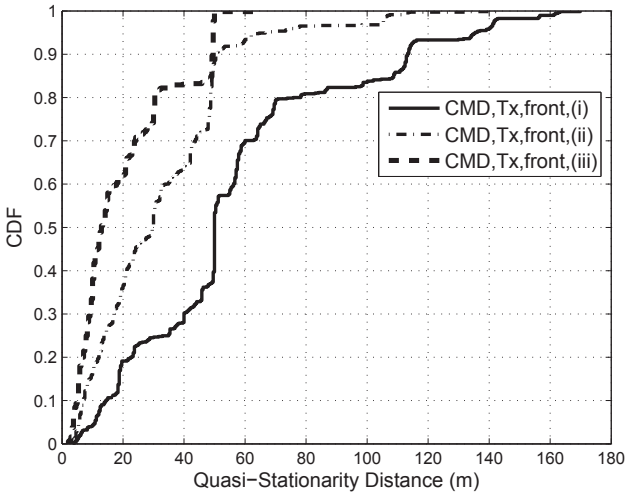

Fig. 15. Impact of electrical array aperture on the estimated quasi-stationarity distance.

approximately [46]:

$$\Delta\theta \simeq \frac{\lambda}{(M-1)\cdot\Delta d}\cdot\frac{1}{|\cos(\theta)|}\ , \tag{17}$$

where θ is an arbitrary direction angle. Eq. (17) shows that case (ii) has a better angular resolution than case (i). This is similar to the results in [13], where it is found that for vehicle-to-infrastructure scenarios, an increase in the antenna spacing yields an increase in the degree of non-stationarity in the spatial domain. Note that according to (17), cases (ii) and (iii) have same angular resolution, however, the inter-element spacing of (ii) is larger than $\lambda/2$, which increases the possibility of ambiguity [47]. Therefore, case (iii) leads to a smaller quasi-stationarity distance than case (ii) in Fig. 15. Here we only show the results of the route in Fig. 3 as an example. Measurements for other routes were verified, though relevant plots are not shown here due to space limitations. Eventually, it is concluded that a large electrical array aperture leads to reduced quasi-stationarity region size.

G. Metrics

Even though the three metrics describe different aspects of channel, they all aim to characterize the WSS on the propagation level. The estimated sizes of quasi-stationarity regions using SD and shadowing metrics are generally close to the estimations of CMD at Rx side, or using full channel correlation matrix cases. Since the Rx of our measurement system has more antennas (leading to larger electrical array aperture) and thus has a better angular resolution for CMD analysis, the comparison among the three metrics shows that: i) SD and shadowing metrics can be used to characterize quasi-stationarity, and are independent on the electrical array aperture; ii) CMD metric is able to show detailed information of quasi-stationarity at Tx and Rx sides respectively. However, it requires a large electrical array aperture to ensure a good accuracy of estimation; iii) the CMD metric with full channel correlation matrix improves the accuracy of estimation, but it also prevents a detailed analysis of the quasi-stationarity region at each side of Tx and Rx; iv) when characterizing the non-WSS, it is suggested to use SD and shadowing metrics for a measurement system with a small electrical array aperture, e.g., $N_{\mathrm{Rx}}\times N_{\mathrm{Tx}}=2\times 2$ or $N_{\mathrm{Rx}}\times N_{\mathrm{Tx}}=4\times 4$, and to use the CMD metric for arrays with large electrical apertures.

V. Conclusion

In this paper, we employ three metrics, correlation matrix distance (CMD), spectral divergence (SD), and shadow fading

This article has been accepted for publication in a future issue of this journal, but has not been fully edited. Content may change prior to final publication. Citation information: DOI 10.1109/TAP.2015.2402291, IEEE Transactions on Antennas and Propagation

TABLE II
MEAN VALUE OF THE EQUIVALENT QUASI-STATIONARITY REGION SIZE IN METER

	CMD Tx Front	CMD Rx Front	CMD Full Front	SD Front	Shadowing Front	CMD Tx Back	CMD Rx Back	CMD Full Back	SD Back	Shadowing Back
S1	31.14	9.75	5.03	5.87	6.82	25.90	7.39	3.44	5.17	7.62
S2	21.29	7.84	3.70	6.78	-	19.87	5.56	2.86	6.86	-
S3	68.86	16.71	10.18	16.15	36.15	88.58	35.21	21.14	14.72	13.26
S4	20.58	6.64	3.64	3.30	3.12	15.61	4.12	2.76	3.75	6.48
S5	17.31	4.53	2.78	4.45	3.80	16.02	3.49	2.49	3.16	4.61

correlation, to characterize the non-WSS of V2V radio channels based on data measured with a 30×4 MIMO sounder at 5.3 GHz in suburban, urban, and underground parking environments. We consider the impact of antenna layout, environment, LOS/NLOS, and speed in the characterization of the non-WSS. The size of the equivalent quasi-stationarity region ranges from 3 to 80 m in different V2V scenarios. It is found that: i) a large electrical array aperture improves the angular resolution and thus results in a smaller estimated quasi-stationarity region; ii) strong LOS and a small difference of speed between a vehicle of interest and surrounding vehicles lead to large quasi-stationarity region; and iii) environments with a large number of scatterers exhibit smaller quasi-stationarity region. Finally, it is suggested to rely SD and shadowing metrics when measurements are conducted with small electrical aperture size of arrays, and to use CMD metric if arrays with large electrical apertures are employed.

For future work, it would be necessary to precisely evaluate V2V system performance by taking into account the non-stationarity of radio channels. It would also be useful to incorporate the quasi-stationarity region into dynamic channel modeling of non-stationary channels, then a more detailed investigation of the physical phenomena from which non-stationarity originates (e.g., "birth and "death of MPC) can be performed.

VI. ACKNOWLEDGMENTS

The authors would like to thank P. Vainikainen, J. Koivunen, and M. Olkkonen for their contributions in the measurement campaign. The authors also wish to express their appreciation to anonymous reviewers for their thorough reading and constructive comments, which greatly helped to improve the paper.

REFERENCES

[1] R. He, O. Renaudin, V.-M. Kolmonen, K. Haneda, Z. Zhong, B. Ai, and C. Oestges, "Non-stationarity characterization for vehicle-to-vehicle channels using correlation matrix distance and shadow fading correlation," in *Proc. 35th Progress In Electromagnetics Research Symposium*, Guangzhou, China, 2014, pp. 1–5.

[2] C. F. Mecklenbräuker, A. F. Molisch, J. Karedal, F. Tufvesson, A. Paier, L. Bernadó, T. Zemen, O. Klemp, and N. Czink, "Vehicular channel characterization and its implications for wireless system design and performance," *Proceedings of the IEEE*, vol. 99, no. 7, pp. 1189–1212, 2011.

[3] P. Bello, "Characterization of randomly time-variant linear channels," *IEEE Transactions on Communications Systems*, vol. 11, no. 4, pp. 360–393, 1963.

[4] A. Paier, J. Karedal, N. Czink, H. Hofstetter, C. Dumard, T. Zemen, F. Tufvesson, A. F. Molisch, and C. F. Mecklenbräuker, "Car-to-car radio channel measurements at 5 GHz: Pathloss, power-delay profile, and delay-Doppler spectrum," in *Proc. IEEE ISWCS'07*, 2007, pp. 224–228.

[5] A. Paier, J. Karedal, N. Czink, H. Hofstetter, C. Dumard, T. Zemen, F. Tufvesson, C. F. Mecklenbräuker, and A. F. Molisch, "First results from car-to-car and car-to-infrastructure radio channel measurements at 5.2 GHz," in *Proc. IEEE PIMRC'07*, 2007, pp. 1–5.

[6] A. F. Molisch, F. Tufvesson, J. Karedal, and C. Mecklenbräuker, "A survey on vehicle-to-vehicle propagation channels," *IEEE Wireless Communications*, vol. 16, no. 6, pp. 12–22, 2009.

[7] D. W. Matolak, "Channel modeling for vehicle-to-vehicle communications," *IEEE Communications Magazine*, vol. 46, no. 5, pp. 76–83, 2008.

[8] G. Matz, "On non-WSSUS wireless fading channels," *IEEE Transactions on Wireless Communications*, vol. 4, no. 5, pp. 2465–2478, 2005.

[9] R. Bultitude, C. Charalambous, X. Li, M. Herben, and G. Brussaard, "Development of a model for realistic portrayal of random time variations on mobile radio channels," in *Proc. URSI General Assembly'02*, Maastricht, the Netherlands, 2002, pp. 2119–2122.

[10] G. Matz, "Characterization of non-WSSUS fading dispersive channels." in *Proc. IEEE ICC'03*, Anchorage, USA, 2003, pp. 2480–2484.

[11] A. Gehring, M. Steinbauer, I. Gaspard, and M. Grigat, "Empirical channel stationarity in urban environments," in *EPMCC'01*, Vienna, Austria, 2001, pp. 1–6.

[12] A. Ispas, G. Ascheid, C. Schneider, and R. Thomä, "Analysis of local quasi-stationarity regions in an urban macrocell scenario," in *Proc. IEEE VTC'10*, Taipei, 2010, pp. 1–5.

[13] A. Ispas, C. Schneider, G. Ascheid, and R. Thomä, "Analysis of the local quasi-stationarity of measured dual-polarized MIMO channels," *IEEE Transactions on Vehicular Technology*, to be published, 2014.

[14] L. Bernadó, "Non-stationarity in vehicular wireless channels," Ph.D. dissertation, Technische Universität Wien, Vienna, Austria, Apr. 2012.

[15] M. Priestley and T. S. Rao, "A test for non-stationarity of time-series," *Journal of the Royal Statistical Society, Series B*, vol. 31, pp. 140–149, 1969.

[16] C. J. Mecklin and D. J. Mundfrom, "An appraisal and bibliography of tests for multivariate normality," *International Statistical Review*, vol. 72, no. 1, pp. 123–138, 2004.

[17] S. Kay, "A new nonstationarity detector," *IEEE Transactions on Signal Processing*, vol. 56, no. 4, pp. 1440–1451, 2008.

[18] N. Henze and B. Zirkler, "A class of invariant consistent tests for multivariate normality," *Communications in Statistics-Theory and Methods*, vol. 19, no. 10, pp. 3595–3617, 1990.

[19] P. Borgnat, P. Flandrin, P. Honeine, C. Richard, and J. Xiao, "Testing stationarity with surrogates: A time-frequency approach," *IEEE Transactions on Signal Processing*, vol. 58, no. 7, pp. 3459–3470, 2010.

[20] T. J. Willink, "Wide-sense stationarity of mobile MIMO radio channels," *IEEE Transactions on Vehicular Technology*, vol. 57, no. 2, pp. 704–714, 2008.

[21] K. V. Mardia, J. T. Kent, and J. M. Bibby, "Multivariate analysis," 1980.

[22] W. Martin, "Measuring the degree of non-stationarity by using the Wigner-Ville spectrum," in *Proc. IEEE ICASSP'84*, San Diego, USA, 1984, pp. 262–265.

[23] A. Ispas, M. Dörpinghaus, G. Ascheid, and T. Zemen, "Characterization of non-stationary channels using mismatched Wiener filtering," *IEEE Transactions on Signal Processing*, vol. 61, no. 2, pp. 274–288, 2013.

[24] M. Herdin, "Non-stationary indoor MIMO radio channels," Ph.D. dissertation, Technische Universität Wien, Vienna, Austria, Aug. 2004.

This article has been accepted for publication in a future issue of this journal, but has not been fully edited. Content may change prior to final publication. Citation information: DOI 10.1109/TAP.2015.2402291, IEEE Transactions on Antennas and Propagation

[25] M. Herdin and E. Bonek, "A MIMO correlation matrix based metric for characterizing non-stationarity," in *Proceedings IST Mobile & Wireless Communications Summit*, 2004.

[26] M. Herdin, N. Czink, H. Özcelik, and E. Bonek, "Correlation matrix distance, a meaningful measure for evaluation of non-stationary MIMO channels," in *Proc. IEEE VTC'05*, vol. 1, 2005, pp. 136–140.

[27] O. Renaudin, V.-M. Kolmonen, P. Vainikainen, and C. Oestges, "Non-stationary narrowband MIMO inter-vehicle channel characterization in the 5-GHz band," *IEEE Transactions on Vehicular Technology*, vol. 59, no. 4, pp. 2007–2015, 2010.

[28] O. Renaudin, V. Kolmonen, P. Vainikainen, and C. Oestges, "Car-to-car channel models based on wideband MIMO measurements at 5.3 GHz," in *Proc. IEEE EuCAP'09*, 2009, pp. 635–639.

[29] A. Paier, T. Zemen, L. Bernadó, G. Matz, J. Karedal, N. Czink, C. Dumard, F. Tufvesson, A. F. Molisch, and C. F. Mecklenbräuker, "Non-WSSUS vehicular channel characterization in highway and urban scenarios at 5.2 GHz using the local scattering function," in *Proc. IEEE ITG WSA'08*, Vienna, Austria, 2008, pp. 9–15.

[30] T. T. Georgiou, "Distances and Riemannian metrics for spectral density functions," *IEEE Transactions on Signal Processing*, vol. 55, no. 8, pp. 3995–4003, 2007.

[31] F. Kaltenberger, L. Bernadó, and T. Zemen, "Characterization of MU-MIMO channels using the spectral divergence measure," *COST 2100, TD (08)*, vol. 640, 2008.

[32] L. Bernadó, T. Zemen, A. Paier, G. Matz, J. Karedal, N. Czink, C. Dumard, F. Tufvesson, M. Hagenauer, A. F. Molisch *et al.*, "Non-WSSUS vehicular channel characterization at 5.2 GHz-spectral divergence and time-variant coherence parameters," *XXIXth URSI General Assembly*, pp. 9–16, 2008.

[33] L. Bernadó, T. Zemen, A. Paier, and J. Karedal, "Complexity reduction for vehicular channel estimation using the filter divergence measure," in *Proc. IEEE ASILOMAR'10*, 2010, pp. 141–145.

[34] M. Gudmundson, "Correlation model for shadow fading in mobile radio systems," *Electronics letters*, vol. 27, no. 23, pp. 2145–2146, 1991.

[35] T. Jamsa, P. Kyosti, and J. Iinatti, "Correlation error metrics of simulated MIMO channels," in *Proc. IEEE VTC'07*, 2007, pp. 407–412.

[36] R. Bultitude, G. Brussaard, M. Herben, and T. Willink, "Radio channel modelling for terrestrial vehicular mobile applications," in *Proc. Millenium Conf. Antennas and Propagation*, 2000, pp. 1–5.

[37] D. Umansky and M. Pätzold, "Stationarity test for wireless communication channels," in *Proc. IEEE GLOBECOM'09*, 2009, pp. 1–6.

[38] V. Kolmonen, J. Kivinen, L. Vuokko, and P. Vainikainen, "5.3-GHz MIMO radio channel sounder," *IEEE Transactions on Instrumentation and Measurement*, vol. 55, no. 4, pp. 1263–1269, 2006.

[39] O. Renaudin, "Experimental channel characterization for vehicle-to-vehicle communication systems," Ph.D. dissertation, Université Catholique de Louvain, Louvain-la-Neuve, Belgium, Aug. 2013.

[40] A. F. Molisch, *Wireless communications 2nd ed.* Wiley, 2010.

[41] A. F. Molisch and M. Steinbauer, "Condensed parameters for characterizing wideband mobile radio channels," *International Journal of Wireless Information Networks*, vol. 6, no. 3, pp. 133–154, 1999.

[42] W. C. Lee, "Estimate of local average power of a mobile radio signal," *IEEE Transactions on Vehicular Technology*, vol. 34, no. 1, pp. 22–27, 1985.

[43] E. Bonek, M. Herdin, W. Weichselberger, and H. Ozcelik, "MIMO-study propagation first!" in *Proc. IEEE ISSPIT'03*, 2003, pp. 150–153.

[44] J. D. Parsons, *The mobile radio propagation channel*. John Wiley New York, 2000.

[45] G. L. Stüber, *Principles of mobile communication*. Springer, 2011.

[46] P. Stoica and R. L. Moses, *Spectral analysis of signals*. Pearson/Prentice Hall Upper Saddle River, NJ, 2005.

[47] H. Krim and M. Viberg, "Two decades of array signal processing research: the parametric approach," *IEEE Signal Processing Magazine*, vol. 13, no. 4, pp. 67–94, 1996.

Ruisi He (S'11-M'13) received the B.E. and Ph.D. degrees from Beijing Jiaotong University, Beijing, China, in 2009 and 2015, respectively.

He is currently an Associate Professor with the State Key Laboratory of Rail Traffic Control and Safety, Beijing Jiaotong University, Beijing, China. From March to September 2010, he has been a Visiting Scholar in Universidad Politécnica de Madrid, Madrid, Spain. From August 2012 to September 2013, he has been a Research Scholar with the Department of Electrical and Engineering, University of Southern California, Los Angeles, CA, USA. From December 2013 to July 2014, he has been a Visiting Scholar with the Institute for Information and Communication Technologies, Université Catholique de Louvain, Louvain, Belgium. His current research interests are in the field of measurement and modeling of wireless propagation channels, high-speed railway and vehicular communications, antennas, and signal processing. He has authored/co-authored over 50 research papers in international journals and conferences.

Dr. He serves as the Early Career Representative (ECR) of Commission C - Radiocommunication Systems and Signal Processing, International Union of Radio Science (URSI), from 2014-2017. He serves as a Technical Program Committee (TPC) chair of "Antenna and wave propagation" for APEMC 2015, and as a TPC member for the IEEE ICC 2015, GLOBECOM 2014, WCNC 2015, VTC 2015, IWCMC 2015, VTC 2014, and IWCMC 2014. He is also a section editor of the section "railway communications" for the upcoming COST IC1004 final book. He received the Best Paper Award in IEEE ICGSIS in 2011, the IBM Excellent Student Award of China in 2013, Siemens China Scholarship Award in 2012, and PhD National Scholarship of China in 2013 and 2014. He is a member of the IEEE and a member of the COST IC1004.

Olivier Renaudin received the Electrical Engineering degrees from the Ecole Nationale Supérieure d'Electronique, Informatique et Radiocommunications de Bordeaux (ENSEIRB) and the Université Bordeaux 1, Bordeaux, France, respectively, in 2006. He then joined the Université catholique de Louvain (UCLouvain), Louvain-la-Neuve, Belgium, where he received the PhD degree in 2013. His doctoral research dealt with the experimental characterization of the radio propagation channel for vehicle-to-vehicle communication systems. Since May 2014, he works as a postdoctoral researcher in the Wireless Devices and Systems Group at University of Southern California (USC), Los Angeles (USA). His current research interests include channel sounding, characterization and modeling as well as high-resolution parameter extraction techniques.

Veli-Matti Kolmonen received the M.Sc. degree in technology from Helsinki University of Technology (TKK), Espoo, Finland, in 2004 and the D.Sc. degree in technology from Aalto University, Espoo, Finland in 2010.

From 2003 to 2012, he was with the Department of Radio Science and Engineering, Aalto University, first as a Research Assistant, then as a Researcher, and finally as a Postdoctoral Researcher. He was with Philips Medical Systems MR Finland, Vantaa, Finland. Currently he is with Nokia Technologies, Finland.

This article has been accepted for publication in a future issue of this journal, but has not been fully edited. Content may change prior to final publication. Citation information: DOI 10.1109/TAP.2015.2402291, IEEE Transactions on Antennas and Propagation

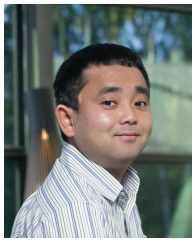

Katsuyuki Haneda received the Doctor of Engineering from the Tokyo Institute of Technology, Tokyo, Japan, in 2007. Dr. Haneda is presently an assistant professor in the Aalto University School of Electrical Engineering. Dr. Haneda was the recipient of the best paper award of the antennas and propagation track in the IEEE 77th Vehicular Technology Conference (VTC2013-Spring), Dresden, Germany, and of the best propagation paper award in the 7th European Conference on Antennas and Propagation (EuCAP2013), Gothenburg, Sweden. Dr. Haneda has been serving as an associate editor for the IEEE Transactions on Antennas and Propagation since 2012 and as an editor for the Antennas, Channel Models, and Location Area of the IEEE Transactions on Wireless Communications since 2013. He also served as a co-chair of the topical working group on indoor environment and has been an active member of the European COST Action IC1004 "Cooperative radio communications for green smart environments". His current research activity focuses on high-frequency radios such as millimeter-wave and beyond, wireless for medical and post-disaster scenarios, radio wave propagation prediction, and in-band full-duplex radio technologies.

Zhangdui Zhong received the B.E. and M.S. degrees from Beijing Jiaotong University, Beijing, China, in 1983 and 1988, respectively. He is a Professor and Advisor of Ph.D. candidates with Beijing Jiaotong University, Beijing, China. He is currently a Director of the School of Computer and Information Technology and a Chief Scientist of State Key Laboratory of Rail Traffic Control and Safety, Beijing Jiaotong University. He is also a Director of the Innovative Research Team of Ministry of Education, Beijing, and a Chief Scientist of Ministry of Railways, Beijing. He is an Executive Council Member of Radio Association of China, Beijing, and a Deputy Director of Radio Association, Beijing. His interests include wireless communications for railways, control theory and techniques for railways, and GSM-R systems. His research has been widely used in railway engineering, such as Qinghai-Xizang railway, Datong-Qinhuangdao Heavy Haul railway, and many high-speed railway lines in China.

He has authored or coauthored seven books, five invention patents, and over 200 scientific research papers in his research area. He received the MaoYiSheng Scientific Award of China, ZhanTianYou Railway Honorary Award of China, and Top 10 Science/Technology Achievements Award of Chinese Universities.

Bo Ai (M'00-SM'10) received the M.S. and Ph.D. degrees from Xidian University, Xi'an, China, in 2002 and 2004, respectively.

He was with Tsinghua University, Beijing, China, where he was an Excellent Postdoctoral Research Fellow in 2007. He is currently a Professor and an Advisor of Ph.D. candidates with Beijing Jiaotong University, Beijing, where he is also the Deputy Director of the State Key Laboratory of Rail Traffic Control and Safety. He is also currently with the Engineering College, Armed Police Force, Xi'an. He has authored or coauthored six books and 140 scientific research papers, and holds 26 invention patents in his research areas. His interests include the research and applications of orthogonal frequency-division multiplexing techniques, high-power amplifier linearization techniques, radio propagation and channel modeling, global systems for mobile communications for railway systems, and long-term evolution for railway systems.

Dr. Ai is a Fellow of The Institution of Engineering and Technology. He was as a Cochair or a Session/Track Chair for many international conferences such as the 9th International Heavy Haul Conference (2009); the 2011 IEEE International Conference on Intelligent Rail Transportation; HSRCom2011; the 2012 IEEE International Symposium on Consumer Electronics; the 2013 International Conference on Wireless, Mobile and Multimedia; IEEE Green HetNet 2013; and the IEEE 78th Vehicular Technology Conference (2014). He is an Associate Editor of IEEE TRANSACTIONS ON CONSUMER ELECTRONICS and an Editorial Committee Member of the Wireless Personal Communications journal. He has received many awards such as the Qiushi Outstanding Youth Award by HongKong Qiushi Foundation, the New Century Talents by the Chinese Ministry of Education, the Zhan Tianyou Railway Science and Technology Award by the Chinese Ministry of Railways, and the Science and Technology New Star by the Beijing Municipal Science and Technology Commission.

Claude Oestges (M'05-SM'12) received the M.Sc. and Ph.D. degrees in Electrical Engineering from the Université catholique de Louvain (UCL), Louvain-la-Neuve, Belgium, respectively in 1996 and 2000. In January 2001, he joined as a post-doctoral scholar the Smart Antennas Research Group (Information Systems Laboratory), Stanford University, CA, USA. From January 2002 to September 2005, he was associated with the Microwave Laboratory UCL as a post-doctoral fellow of the Belgian Fonds de la Recherche Scientifique (FRS-FNRS). Claude Oestges is presently Associate Professor with the Electrical Engineering Department, Institute for Information and Communication Technologies, Electronics and Applied Mathematics, UCL. He also currently serves as an Associate Editor for the IEEE Transactions on Antennas and Propagation and the IEEE Transactions on Vehicular Technology. He is the author or co-author of three books and more than 180 journal papers and conference communications, and was the recipient of the 1999-2000 IET Marconi Premium Award and of the IEEE Vehicular Technology Society Neal Shepherd Award in 2004 and 2012.